

Quasigraphite: Density functional theory based predictions of a structure and its properties

M. G. Ganchenkova, T. T. Vehviläinen, and R. M. Nieminen
Laboratory of Physics, Helsinki University of Technology, P.O. Box 1100, 02015, Finland
 (Received 4 October 2008; published 20 November 2008)

Based on density-functional calculations, we propose a carbon-based nanostructure which we call quasigraphite phase. The quasigraphite phase resembles carbon nanotubes welded into planes, which are arranged similar to layers in graphite. It demonstrates a strong stability with respect to temperatures and external strain. The elastic and electronic properties of the proposed structure are discussed.

DOI: [10.1103/PhysRevB.78.195421](https://doi.org/10.1103/PhysRevB.78.195421)

PACS number(s): 61.48.-c, 61.43.Bn, 61.66.-f, 64.70.Nd

Various kinds of carbon structures exist in nature or have been synthesized in experiments.¹ The well-known structures are diamond, which is the nature's hardest material, and graphite, which is very soft in shear even though the bonds between atoms within the sheets are extremely strong. The discovery of carbon nanotubes² and fullerenes³ as well as recent graphene studies has intensified the interest toward carbon materials.

In particular, there has been growing interest in creating fullerene based polymers as possible candidates for superconductors,⁴ strong and light materials, hydrogen storage materials,⁵⁻⁷ quantum dots,^{8,9} and biological applications.^{10,11} In this respect C_{60} -based polymers have been studied intensively.^{12,13} However recent synthesis of a broad variety of fullerene cages has made it also possible to design various kinds of polymers with other kinds of fullerenes as alternative building blocks.

Among different fullerenes, the smallest one, C_{20} , seems very promising for polymer creation. Indeed, while carbon atoms in C_{20} molecule exhibit sp^2 hybridization, as typical for fullerenes in general, the extreme curvature of the cage surface makes the dihedral angles between bonds more appropriate to sp^3 hybridization. One should expect that for C_{20} the change of the hybridization type, which is a prerequisite for chemical bonding between fullerenes during polymerization, is especially easy, and hence C_{20} should manifest extreme reactivity and easily form compounds. However, so far only one three-dimensional (3D) C_{20} -based polymer has been experimentally produced.^{14,15} Based on the comparison of computational and experimental Raman and IR spectra Iqbal *et al.*¹⁴ have shown that the best fit to the experimental data is demonstrated by face-centered-cubic (fcc) C_{22} structure, where C_{20} molecules are located in face-centered-cubic lattice bound by two additional C atoms. According to computational studies other stable 3D polymer structures might exist, including various simple-cubic (sc),^{4,16} fcc,¹⁶ and body-centered-cubic (bcc) (Refs. 16 and 17) phases.

Following this trend we have been studying the formation of different C_{20} -based polymer structures. The equilibrium configurations and energies of different polymer structures are determined using the spin-polarized density-functional theory (DFT) (Refs. 18 and 19) within the generalized gradient approximation (GGA) implemented in VASP code.^{20,21} In order to describe the carbon ion core electrons, the projector augmented wave (PAW) potential^{22,23} is used. In order to represent C_{20} polymers, calculation supercells usually contain 20 atoms. The supercell shapes are selected so that the

cell repetition due to periodic boundary condition provides the desired overall polymer lattice symmetry. The relaxation of atomic positions is performed with molecular statics method. The kinetic-energy cutoff of 400 eV with $6 \times 6 \times 6$ Brillouin-zone sampling is applied. We have checked that these values provide the convergence of the supercell total energy within 10 meV.

A typical simulation scheme involves the arrangement of C_{20} molecules in a desirable lattice structure at sufficiently large intermolecular separations, followed by gradual decrease in intermolecular separations (structure compression) until the molecules become bound to each other and form two- or three-dimensional structures. In this way, we have systematically studied the most reasonable structures, which can be created using 20 atom supercell, namely—sc, fcc, bcc, and hexagonal closed packed. In all considered cases the polymer formation was found to require no activation barrier, in agreement with the earlier findings of Okada *et al.*¹⁷ As a result we have found several equilibrium C_{20} -based polymer structures.²⁴

In order to test their stability with respect to the action of compressive loads, both isotropic and anisotropic strains were applied to the considered structures. In one of these computational experiments, we have observed a pressure induced phase transformation of one of the stable polymers to a completely different structure, which we have named the “quasigraphite phase” (QGP) (Fig. 1). The scheme of QGP generation is shown in Fig. 2. According to the general scheme described above, the fullerene cages are initially packed in a simple-cubic lattice, facing each other with par-

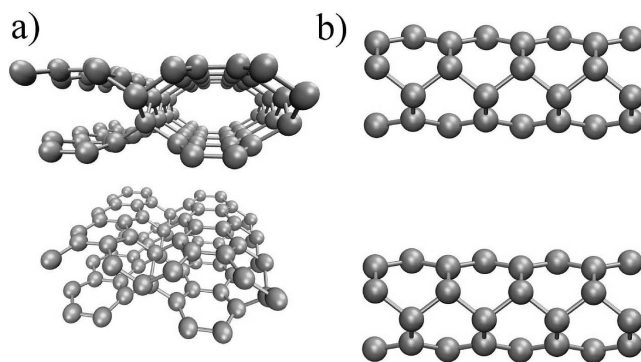


FIG. 1. In the quasigraphite structure, small tubes are joined together forming layers. Atoms are sp^2 hybridized except atoms which join tubes together.

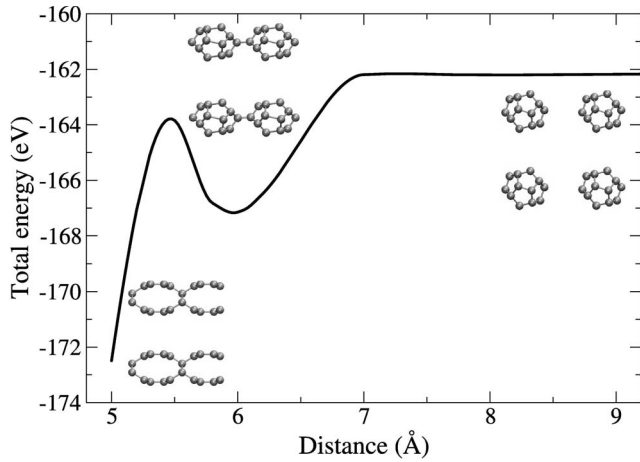


FIG. 2. The pressure induced phase transformation of the C_{20} -based layered cubic structure. Here, the distance means the size of the supercell, which contains only one C_{20} .

allel edges (the rightmost inset of Fig. 2). Gradual isotropic compression of this system eventually results in the equilibrium layered sc polymer structure with the lattice parameter of 6 Å, as shown in the middle inset of Fig. 2. If, however, the hydrostatic compression is continued, another phase transformation takes place when the pressure reaches the value of 30 GPa (see Fig. 2) and a high-pressure phase, which is QGP, is formed. The activation barrier associated with the transition is about 3 eV/fullerene.

The resulting structure, which is characterized by the cohesive energy of 8.91 eV/atom, is not only more energetically favorable than the intermediate sc structure but turned out to have the largest cohesive energy among all the equilibrium 3D polymers based on C_{20} (see Table I and Ref. 24). Note that the transition is induced exclusively by application of pressure without any assistance of temperature (the latter is always zero for the molecular static relaxation used here).

The structure of quasigraphite phase can be described as an arrangement of *nanotubes* welded together in planar layers, which are, in turn, stacked in a graphitelike manner. The atoms that provide nanotube “welding” manifest the sp^3 hybridization while the others constituting the nanotubes have

sp^2 hybridization. Correspondingly, the quasigraphite phase is characterized by two different sets of bond lengths (Table I): those corresponding to the diamondlike sp^3 -type bonds (with the bond length of about 1.54 Å) and those corresponding to graphitelike sp^2 hybridized bonds (1.42 Å).

Thus the quasigraphite phase consists of two-dimensional layers of packed nanotubes while the layer arrangement and interlayer separations are similar to those observed for individual carbon sheets in graphite. The latter indicates that the interaction between layers is, like in graphite, due mostly to van der Waals (vdW) forces. Correspondingly, the interlayer separation predicted by DFT should be taken with caution because vdW interaction is known to be treated improperly in this case. In order to improve the description of vdW interaction, the obtained equilibrium QGP structure was re-optimized using CPMD code,²⁵ which allows estimation of the additive vdW contribution E_{vdw} to the standard DFT energies using an empirical damped dispersion force model^{26,27}

$$E_{\text{vdw}} = \sum_{ij} \frac{C_6^{\alpha\beta}}{R_{ij}^{\alpha\beta 6}} \left(1 - \exp \left[-d \left(\frac{R_{ij}^{\alpha\beta}}{R_0^{\alpha\beta}} \right)^7 \right] \right)^4. \quad (1)$$

In this formula $C_6^{\alpha\beta}$ is the diatomic vdW force coefficient, $R_0^{\alpha\beta}$ is the sum of the vdW radii of two interacting atoms, $R_{ij}^{\alpha\beta}$ is the distance between atoms, and d is the damping coefficient. This model ensures that bonded interactions are not included since the effect of vdW correction drops to zero when the distance between atoms is about 3 Å. In the current calculations we used the set of parameters appropriate for this model, as obtained by Williams and Malhotra²⁸ using Perdew-Burke-Ernzerhof (PBE) and Becke-Lee-Yang-Parr (BLYP) functionals.

The application of vdW corrections resulted in the optimized distance between QGP planes of 3.0 Å (see Fig. 3). For comparison, the same procedure that was repeated for graphite predicted the graphite interlayer distance of 3.1 Å. This value differs from the experimental one, 3.35 Å, by less than 10%, giving a rough estimate of the accuracy of interplane separation determination for QGP as well.

Next, we present the results of elastic and electronic property calculations for the quasigraphite phase. In order to cal-

TABLE I. Energies and lattice parameters for QGP in comparison with well-known carbon structures. In QGP lattice vector c is perpendicular to the layer. Energies are given without vdW energy taken into account.

Structure	E/atom (eV)	E/atom ^a (eV)	Lattice vectors	Bond lengths (Å)
Diamond	-9.10	-9.22	$a=3.573$ Å	1.54
Graphite	-9.25	-9.24	$a=b=2.46$ Å, $c=6.2$ Å	1.42
C_{20} fullerene	-8.07	-8.01		1.45
C_{20} sc	-8.36		$a=6.06$ Å, $b=5.86$ Å, $c=6.48$ Å	1.38, 1.42, 1.33, 1.48 1.52, 1.53, 1.55, 1.66
C_{20} fcc	-8.79		$a_1=[4.31, 4.54, 0.32]$ Å $a_2=[0.32, 4.54, 4.31]$ Å $a_3=[3.98, 0.65, 3.98]$ Å	1.34, 1.50, 1.53, 1.54 1.56, 1.57
C_{20} QGP	-8.91		$a=4.91$ Å, $b=5.36$ Å, $c=6.0$ Å	1.41, 1.46, 1.51, 1.55

^aReference 16.

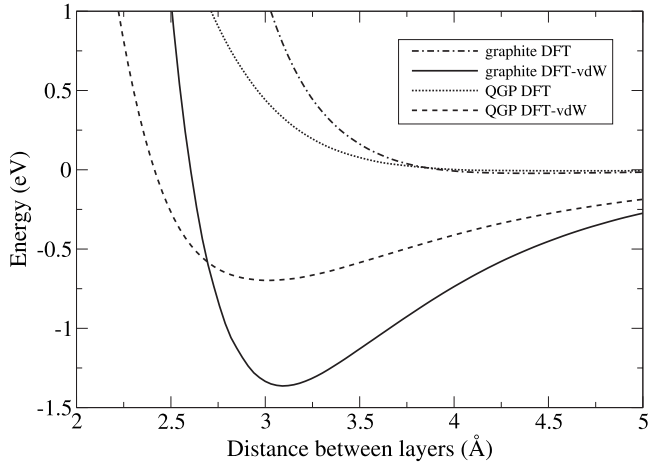


FIG. 3. The dependence of the binding energy between layers for 20 atom supercell for quasigraphite phase and graphite vs the distance between layers when van der Waals correction is taken into account.

culate elastic properties after structural optimization of QGP, small distortions to its equilibrium lattice vectors were applied. Then from the distortions and corresponding energies, the elastic constants were deduced. For this purpose the procedure described in the paper by Ravindran *et al.*²⁹ was used.

The bulk modulus was calculated using the Murnaghan equation of state³⁰

$$E(V) = \frac{BV}{B'(B'-1)} \left[B' \left(1 - \frac{V_0}{V} \right) + \left(\frac{V_0}{V} \right)^{B'} - 1 \right] + E_0, \quad (2)$$

where V_0 is equilibrium volume, B' is pressure derivative of the bulk modulus, and E_0 is the equilibrium energy. The calculated elastic constants and bulk modulus are presented in Table II. The elastic constants c_{11} and c_{33} for QGP, graphite, and carbon nanotubes are found to be very similar, as could be expected since their geometries are similar in the strain direction. The difference between calculated values of the bulk modulus and experimental values is small, less than 3% for solids and 10% for layered materials.

TABLE II. Elastic properties of QGP in comparison with the well-known carbon structures.

Structure	Method	c_{11} (GPa)	c_{22} (GPa)	c_{33} (GPa)	c_{44} (GPa)	c_{66} (GPa)	c_{12} (GPa)	B (GPa)
Diamond	this study	1085			569		140	447
	experimental ^a	1079			575		124	442
Graphite	this study	1058		49				39
	experimental ^b	1060		36				34
Nanotube	empirical ^c	1060		40				19
C_{20} QGP	this study	1050	636	49		340	90	50

^aReference 34.

^bReference 35.

^cReference 36.

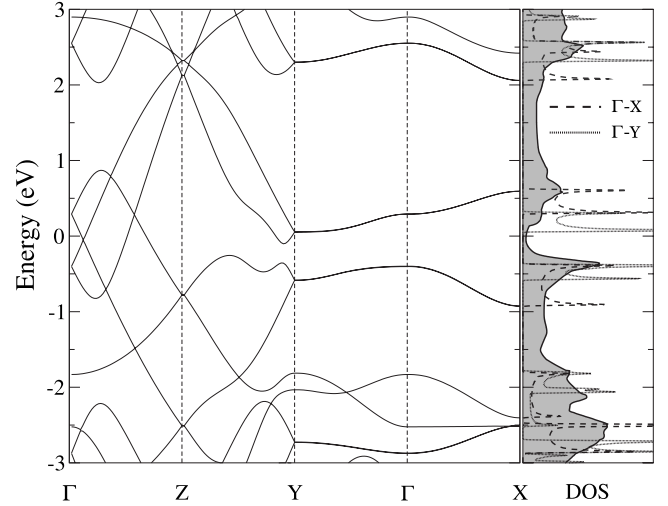


FIG. 4. In the DOS plot, filled curve is the total DOS for QGP while $\Gamma-X$ and $Y-\Gamma$ sections are plotted separately. For clarity DOS curves are scaled.

The calculations of electronic structure show that QGP structure manifests metallic properties along the axis of the tube and no metallic conductivity in in-plane ($\Gamma-X$) and perpendicular ($Y-\Gamma$) directions [see the band structure and electronic density of states (DOS) shown in Fig. 4]. This behavior is to some extent similar to that for graphite. However, in contrast to the graphite electronic structure, for QGP there are two well localized states in ($\Gamma-X$) and ($Y-\Gamma$) directions seen in the band gap. Moreover, in order to excite an electron from the lowest of these localized states, which is fully occupied, to the next empty level, one needs only 0.69 and 0.40 eV in ($\Gamma-X$) and ($Y-\Gamma$) directions, respectively. This electronic band property can possibly be used in applications which require photons with high frequency.

To examine the stability of the QGP structure, we have performed molecular dynamic simulations using CPMD (Ref. 25) code with the Parrinello-Rahman³¹ constant-temperature constant pressure (NPT) technique and the GGA. The size of the supercell for the stability studies was 160 atoms and Brillouin-zone sampling was done with the Γ point.

Both isotropic and anisotropic strains were considered. It is found that the QGP structure endures pressures up to 50

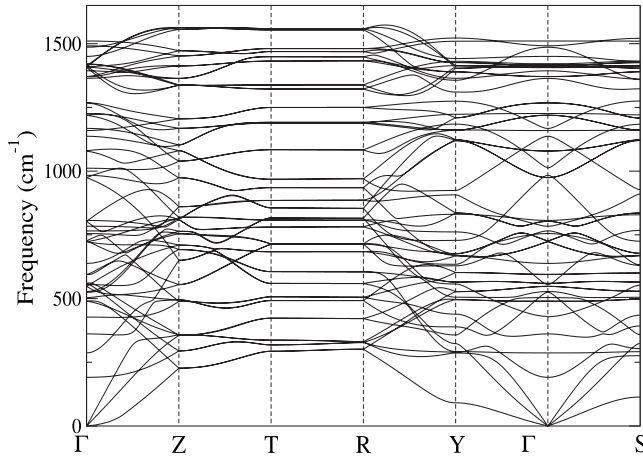


FIG. 5. Phonon dispersion relations for QGP show absence of zero-mode components which promotes stability of the structure.

GPa without any phase transformations. At higher pressures, however, a phase transformation may occur. In particular, a shock induced phase transformation takes place when the pressure is rapidly increased to values higher than 50 GPa. In this case bonds between quasigraphite sheets are formed and the structure transforms to the phase which can be considered as amorphous diamond. The structures which are energetically less favorable such as cubic structures undergo phase transformations much easier than QGP structure. However even they are highly resistant against external strains and high temperatures, remaining stable up to 20 GPa and 1000 K.

The stability of the QGP structure is also confirmed by the absence of the zero-mode components in the calculated phonon-dispersion spectrum (Fig. 5), which was calculated using finite difference approach implemented in ABINIT code within local-density approximation (LDA). In order to estimate the sensitivity of calculated frequencies to the choice of the exchange-correlation approximation and the code used, the phonon modes were calculated using both LDA and GGA, and VASP. In all tested cases, GGA gives approximately 50 cm^{-1} lower frequencies than LDA, which correlates with the known fact that LDA overestimates interatomic binding, whereas GGA underestimates it. With LDA, VASP gives the same results as ABINIT.

Since vibrational information is very sensitive to the spatial disposition of chemical bonds in an atomic structure, Raman spectroscopy provides a fingerprint by which the studied structure can be identified. Therefore we have calculated Raman spectra for QGP which can be used by experimentalists for its identification if synthesized. Raman intensities are calculated within LDA approximation using ABINIT. The dynamical matrices are calculated with a $4 \times 4 \times 4$ grid of special high-symmetry q points and 680 eV kinetic-energy cutoff for the plane waves. ABINIT uses density-functional perturbation theory and linear-response functions to calculate intensities. Linear response calculations give Raman susceptibility tensor R , whose elements are derivatives of polarizability. The intensity of a phonon mode is proportional to the largest eigenvalue of R^*R . A mode is Raman active only if the motion occurs with a changing polarizability. At some

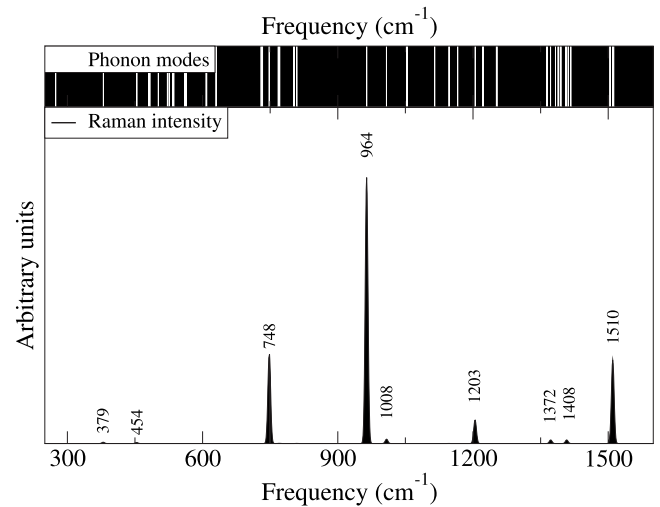


FIG. 6. Phonon modes and Raman spectra for QGP calculated with ABINIT and LDA. The most intense peaks corresponding to Raman-active modes are located at frequencies 748, 964, 1203, and 1510 cm^{-1} , these peaks are distinctive features of QGP and are not seen in any other C_{20} polymer structure studied so far.

distance Δr away from the equilibrium structure, the polarization α is given by

$$\alpha = \alpha_0 + \left(\frac{\partial \alpha}{\partial r} \right) \Delta r, \quad (3)$$

where the term $\frac{\partial \alpha}{\partial r}$ is the change in polarizability with change in nuclear position. If derivative is zero, no Raman scattering occurs. Raman spectra for QGP are presented in Fig. 6. Raman-active modes with noticeable intensity are located at 379, 454, 748, 964, 1008, 1203, 1372, 1408, and 1510 cm^{-1} . Experimental Raman spectra for graphite demonstrate intense peak at 1580 cm^{-1} (G band) and defect band at 1355 cm^{-1} (D band), which is ascribed to defects in carbon aromatic structure.³² In QGP the Raman spectra peak at 1510 cm^{-1} corresponds to G band of graphite but peaks at 748 and 964 cm^{-1} have larger intensity compared to peak at 1510 cm^{-1} . These peaks are fingerprints that are lacking in other C_{20} polymer structures. There are also small peaks at 372 and 1408 cm^{-1} close to D band in graphite.

Summing up, in this paper we propose a carbon structure that we called quasigraphite. The generated structure is reproducible by different *ab initio* computational methods and codes. Moreover it is very stable against external strain and high temperatures. The high stability of the structure leads us to the conclusion that QGP can be synthesized experimentally. Electronic density of states, band structure, and elastic properties has been calculated. Phonon modes manifest stability of the structure and calculated Raman spectra can be used for structure identification in experimental research. We suggest that one of the recipes can be its generation from the layered cubic structure by the slow external isotropic loading by 30–46 GPa at low temperatures. Following the similarities between the quasigraphite phase and both carbon nanotubes and grapheme, one could expect a number of promising properties of the structure.

We wish to thank I. Degtyarenko for the testing of QGP structure with the GAUSSIAN code. This work was supported by the Academy of Finland through Project No. SA120004 and in the framework of the Center of Excellence Program (2006–2011). We are grateful to the Center of Scientific

Computing (CSC) and DEISA Extreme Computing Initiative (DECI) for generous computational resources. The pictures of the molecular structures were drawn using VMD (Ref. 33) visualization package.

-
- ¹H. Terrones and M. Terrones, *New J. Phys.* **5**, 126 (2003).
²S. Iijima, *Nature (London)* **354**, 56 (1991).
³H. Kroto, J. Heath, S. O'Brien, and R. Smalley, *Nature (London)* **318**, 162 (1985).
⁴Y. Miyamoto and M. Saito, *Phys. Rev. B* **63**, 161401(R) (2001).
⁵Y.-H. Kim, Y. Zhao, A. Williamson, M. J. Heben, and S. B. Zhang, *Phys. Rev. Lett.* **96**, 016102 (2006).
⁶Y. Zhao, Y.-H. Kim, A. C. Dillon, M. J. Heben, and S. B. Zhang, *Phys. Rev. Lett.* **94**, 155504 (2005).
⁷Y. X. Ren, T. Y. Ng, and K. M. Liew, *Carbon* **44**, 397 (2006).
⁸S.-H. Ke, H. U. Baranger, and W. Yang, *Phys. Rev. Lett.* **91**, 116803 (2003).
⁹A. S. Alexandrov, A. M. Bratkovsky, and R. S. Williams, *Phys. Rev. B* **67**, 075301 (2003).
¹⁰Y. Tabata and Y. Ikada, *Pure Appl. Chem.* **71**, 2047 (1999).
¹¹W. Noon, Y. Kong, and J. Ma, *Proc. Natl. Acad. Sci. U.S.A.* **99**, 6466 (2002).
¹²S. Okada and A. Oshiyama, *Phys. Rev. B* **68**, 235402 (2003).
¹³T. A. Beu, J. Onoe, and A. Hida, *Phys. Rev. B* **72**, 155416 (2005).
¹⁴Z. Iqbal, Y. Zhand, H. Grebel, S. Vijayalakshmi, A. Lahamer, G. Benedek, M. Bernasconi, J. Cariboni, I. Spagnolatti, R. Sharma, R. F. J. Owens, M. E. Kozlov, K. V. Rao, and M. Muhammed, *Eur. Phys. J. B* **31**, 509 (2003).
¹⁵I. Spagnolatti, M. Bernasconi, and G. Benedek, *Europhys. Lett.* **59**, 572 (2002).
¹⁶Z. Chen, T. Heine, J. Jiao, A. Hirsch, W. Thiel, and P. Schleyer, *Chem.-Eur. J.* **10**, 963 (2004).
¹⁷S. Okada, Y. Miyamoto, and M. Saito, *Phys. Rev. B* **64**, 245405 (2001).
¹⁸P. Hohenberg and W. Kohn, *Phys. Rev.* **136**, B864 (1964).
¹⁹W. Kohn and L. J. Sham, *Phys. Rev.* **140**, A1133 (1965).
²⁰G. Kresse and J. Furthmüller, *Phys. Rev. B* **54**, 11169 (1996).
²¹G. Kresse and J. Furthmüller, *Comput. Mater. Sci.* **6**, 15 (1996).
²²G. Kresse and D. Joubert, *Phys. Rev. B* **59**, 1758 (1999).
²³P. E. Blöchl, *Phys. Rev. B* **50**, 17953 (1994).
²⁴T. Vehviläinen, M. Ganchenkova, and R. Nieminen (unpublished).
²⁵CPMD, Copyright IBM Corp 1990-2006, Copyright MPI für Festkörperforschung Stuttgart, 1997-2001.
²⁶M. Elstner, P. Hobza, T. Frauenheim, and S. Suhai, *J. Chem. Phys.* **114**, 5149 (2001).
²⁷W. Mooij, B. van Eijck, and J. Kroon, *J. Phys. Chem. A* **103**, 9883 (1999).
²⁸R. W. Williams and D. Malhotra, *Chem. Phys.* **327**, 54 (2006).
²⁹P. Ravindran, L. Fast, A. Korzhavyi, and B. Johansson, *J. Appl. Phys.* **84**, 4891 (1998).
³⁰F. Murnaghan, *Proc. Natl. Acad. Sci. U.S.A.* **30**, 244 (1944).
³¹M. Parrinello and A. Rahman, *Phys. Rev. Lett.* **45**, 1196 (1980).
³²S. Reich and C. Thomsen, *Philos. Trans. R. Soc. London, Ser. A* **362**, 2271 (2004).
³³W. Humphrey, A. Dalke, and K. Schulten, *J. Mol. Graphics* **14**, 33 (1996).
³⁴H. McSkimin and P. Andreatch, *J. Appl. Phys.* **43**, 2944 (1972).
³⁵A. A. Ahmadiéh and H. A. Rafizadeh, *Phys. Rev. B* **7**, 4527 (1973).
³⁶J. P. Lu, *Phys. Rev. Lett.* **79**, 1297 (1997).